THE JOURNAL OF BIOLOGICAL CHEMISTRY VOL. 284, NO. 45, pp. 30742–30753, November 6, 2009

Two Pathways for Cyclooxygenase-2 Protein Degradation *in Vivo*[*] [S]

Received for publication, August 4, 2009, and in revised form, September 11, 2009 Published, JBC Papers in Press, September 16, 2009, DOI 10.1074/jbc.M109.052415

Masayuki Wada[‡], Thomas L. Saunders[§], Jason Morrow[¶‖], Ginger L. Milne[¶‖], Kimberly P. Walker[¶‖], Sudhansu K. Dey[**], Thomas G. Brock[§], Mark R. Opp[‡‡], David M. Aronoff[§], and William L. Smith[‡1]

From the Departments of [‡]Biological Chemistry, [‡‡]Anesthesiology, and [§]Internal Medicine, University of Michigan, Ann Arbor, Michigan 48109, the Departments of [¶]Pharmacology and [‖]Medicine, Vanderbilt University, Nashville, Tennessee 37232, and the [**]Division of Reproductive Sciences, The Perinatal Institute, Cincinnati Children's Hospital Medical Center, University of Cincinnati College of Medicine, Cincinnati, Ohio 45229

COX-2, formally known as prostaglandin endoperoxide H synthase-2 (PGHS-2), catalyzes the committed step in prostaglandin biosynthesis. COX-2 is induced during inflammation and is overexpressed in colon cancer. *In vitro*, an 18-amino acid segment, residues 595–612, immediately upstream of the C-terminal endoplasmic reticulum targeting sequence is required for *N*-glycosylation of Asn[594], which permits COX-2 protein to enter the endoplasmic reticulum-associated protein degradation system. To determine the importance of this COX-2 degradation pathway *in vivo*, we engineered a *del*595–612 PGHS-2 (Δ18 COX-2) knock-in mouse lacking this 18-amino acid segment. Δ18 COX-2 knock-in mice do not exhibit the renal or reproductive abnormalities of COX-2 null mice. Δ18 COX-2 mice do have elevated urinary prostaglandin E_2 metabolite levels and display a more pronounced and prolonged bacterial endotoxin-induced febrile response than wild type (WT) mice. Normal brain tissue, cultured resident peritoneal macrophages, and cultured skin fibroblasts from Δ18 COX-2 mice overexpress Δ18 COX-2 relative to WT COX-2 expression in control mice. These results indicate that COX-2 can be degraded via the endoplasmic reticulum-associated protein degradation pathway *in vivo*. Treatment of cultured cells from WT or Δ18 COX-2 mice with flurbiprofen, which blocks substrate-dependent degradation, attenuates COX-2 degradation, and treatment of normal mice with ibuprofen increases the levels of COX-2 in brain tissue. Thus, substrate turnover-dependent COX-2 degradation appears to contribute to COX-2 degradation *in vivo*. Curiously, WT and Δ18 COX-2 protein levels are similar in kidneys and spleens from WT and Δ18 COX-2 mice. There must be compensatory mechanisms to maintain constant COX-2 levels in these tissues.

There are two prostaglandin endoperoxide H synthases (PGHSs)[2] called PGHS-1 and PGHS-2. The enzymes are commonly referred to as COX-1 and COX-2, and we use this latter terminology here. COXs catalyze the committed step in prostanoid biosynthesis, which is the conversion of one molecule of arachidonic acid, two O_2 molecules, and two electrons to prostaglandin endoperoxide H_2 (1–4). PGH_2 is the immediate precursor of what are considered to be the major bioactive prostaglandins (PGs), including PGD_2, PGE_2, $PGF_{2\alpha}$, PGI_2, and thromboxane A_2. A different gene encodes each COX isoform (5–7).

In general, COX-1 is expressed constitutively, and COX-2 is expressed inducibly in response to various stimuli (6, 7). However, COX-2 is expressed constitutively in kidney (8) and brain (9). Each COX isoform subserves a distinct set of biologies (10–12). Both the enzymatic properties and the patterns of expression of the isoforms contribute to their unique functions (12). In part because of the association of COX-2 expression with pathologies such as inflammation and colon cancer (13–15), many studies have been performed to elucidate the mechanisms of transcriptional regulation of COX-2 as reviewed recently (6, 7). It is now also clear that COX-2 is regulated post-transcriptionally at the level of both mRNA degradation (16) and protein degradation (17, 18).

In vitro studies with cultured murine NIH 3T3 fibroblasts and with HEK293 cells heterologously expressing various forms of COX-2 have suggested that there are two independent pathways of COX-2 protein degradation (17, 18) dubbed "endoplasmic reticulum-associated degradation" (ERAD) and "substrate-dependent degradation" pathways. *N*-Glycosylation of Asn[594], which appears to occur post-translationally, leads to entry of COX-2 into the ERAD pathway. Sequences both upstream and downstream of Asn[594] modulate the rate of Asn[594] glycosylation and collectively include a 27-amino acid instability motif (27-IM) involving residues Glu[586] to Lys[612] (18). The second COX-2 degradation process is substrate turnover-dependent,

* This work was supported, in whole or in part, by National Institutes of Health Grants GM 068848 (to W. L. S.), HL085149 (to W. L. S.), HL078727 (to D. M. A.), DK48831 (to G. L. M.), GM15431 (to G. L. M.), HL080972 (to M. R. O.), GM067189 (to M. R. O.), HD012304 (to S. K. D.), and CA77839 (to S. K. D.).

[S] The on-line version of this article (available at http://www.jbc.org) contains supplemental "Experimental Procedures," Figs. S-1 to S-4, Table S-1, and additional references.

[1] To whom correspondence should be addressed: Dept. of Biological Chemistry, University of Michigan Medical School, 1150 W. Medical Center Dr., 5301 MSRB III, Ann Arbor, MI 48109-5606. Tel.: 734-647-6180; Fax: 734-763-4581; E-mail: smithww@umich.edu.

[2] The abbreviations used are: PGHS, prostaglandin endoperoxide H synthase; PG, prostaglandin; COX, cyclooxygenase; DMEM, Dulbecco's modified Eagle medium; MEM, minimum essential medium; FBS, fetal bovine serum; HFBS, heat-inactivated fetal bovine serum; LPS, *E. coli* lipopolysaccharide; CHX, cycloheximide; KIF, kifunensine; mu, murine; PBS, phosphate-buffered saline; FBP, flurbiprofen; WT, wild type (*i.e.* native); Δ18, *del*585–612; ES, embryonic stem cell; ERAD, endoplasmic reticulum-associated degradation; 27-IM, 27-amino acid instability motif; mu, murine.

correlates with COX-2 suicide inactivation, and is independent of *N*-glycosylation at Asn^{594}. *In vitro,* this pathway can be attenuated or blocked by various nonspecific and nonsteroidal anti-inflammatory drugs and COX-2 inhibitors (3, 18). The biochemical mechanism underlying the disappearance of immunoreactive COX-2 associated with substrate-dependent inactivation is unresolved.

Although there is considerable evidence that COX-2 can be degraded by both ERAD and suicide pathways *in vitro*, the relative importance of these processes in COX-2 protein homeostasis *in vivo* has not been determined. To address this issue, we developed a knock-in *del*595–612 PGHS-2 (Δ18 COX-2) mouse in which residues 595–612 are deleted. Absent key residues important in Asn^{594} glycosylation, Δ18 COX-2 cannot undergo degradation via the ERAD pathway. However, Δ18 COX-2 is kinetically and pharmacologically indistinguishable from native COX-2 (17), and like native COX-2 it undergoes a substrate-dependent disappearance (18). Here, we provide evidence that both inactivation processes function *in vivo* in normal and endotoxin-treated mice but that the contribution of each process to COX-2 protein degradation is different in different tissues.

EXPERIMENTAL PROCEDURES

Materials—129X1/SvJ genomic DNA (stock number 000691) was obtained from The Jackson Laboratory. The Expand Long Template PCR system, Complete EDTA-free protease inhibitor mixture, and endoglycosidase H were purchased from Roche Applied Science. QuikChange™ site-directed mutagenesis kit was obtained from Stratagene. Ex Taq™ DNA polymerase (TAK_RR001) was purchased from Takara Mirus Bio. Dulbecco's modified Eagle's medium (DMEM), minimum essential medium (MEM), RPMI 1640 medium, heat-inactivated fetal bovine serum (HFBS), penicillin/streptomycin, Lipofectamine 2000 reagent, Opti-MEM medium, tetracycline, collagenase type II, and NuPAGE were obtained from Invitrogen. Collagenase type A, *Escherichia coli* lipopolysaccharide (LPS), and protease inhibitors were purchased from Sigma. Cycloheximide (CHX) and MG132 were obtained from Calbiochem. Kifunensine (KIF) was purchased from Toronto Research Chemicals. *S*-Flurbiprofen and arachidonic acid were obtained from Cayman Chemical Co. DNeasy blood and tissue kit and RNeasy kit were obtained from Qiagen. [1-^{14}C]Arachidonic acid (1.85 GBq/mmol) was purchased from American Radiolabeled Chemical. Precoated silica gel 60 glass plates for TLC were obtained from Merck. Mouse anti-actin antibody was purchased from MP Biomedicals. Fluorescein isothiocyanate-labeled goat anti-rabbit IgG and goat anti-mouse IgG were obtained from Bio-Rad.

Affinity-purified peptide-specific polyclonal primary antibodies were generated as described previously (19). Antibodies to muCOX-1 prepared against the epitope Leu^{271}–Ala^{285} were used for detection of muCOX-1 by immunoblotting. muCOX-2 antibody against the epitope Gln^{583}–Asn^{594} was used for detection of native and Δ18 muCOX-2 proteins. muCOX-2 antibody against the epitope Ser^{598}–Lys^{612} was used to detect muCOX-2 but not Δ18 muCOX-2. Other antibodies reactive with both muCOX-2 and Δ18 muCOX-2 were obtained from Novus Biological, Inc. (catalog number NB 100-689), and used for tissue immunoblotting.

SDS-PAGE and Western Blotting—Frozen cell pellets or solubilized microsomes prepared from mouse tissue were used as the source of protein for Western blotting. Frozen cell pellets were lysed in 20 mM Tris-HCl, pH 7.4, containing 150 mM NaCl, 2 mM EDTA, 1% Nonidet P-40, 50 mM NaF, 10% glycerol, and a mixture of protease inhibitors (Roche Applied Science) for 10 min on ice. Insoluble material was removed by centrifugation at 16,000 × *g* at 4 °C for 20 min. Protein concentrations were determined using a Pierce BCA protein assay kit. Proteins were separated by electrophoresis on 4–12% polyacrylamide gradient gels or 7% Tris acetate polyacrylamide gels (Invitrogen). For immunoblotting, the proteins were electroblotted onto a polyvinylidene fluoride membrane with a semi-dry blotter (Bio-Rad). The membranes were washed (blocked) overnight in 25 mM Tris-HCl, pH 7.4, containing 0.8% NaCl, 0.02% KCl, 0.1% Tween 20 (TBS-T), and 5% skim milk. The membranes were then incubated with appropriate antibodies against COX-1, COX-2, or actin for 2 h. After the membrane had been rinsed three times for 10 min with TBS-T containing 1% skim milk, it was incubated with goat anti-rabbit or goat anti-mouse horseradish peroxidase-conjugated secondary antibodies (Bio-Rad) for 1 h. After washing four times for 10 min with TBS-T, immunodetection was performed using a Pierce SuperSignal West Pico chemiluminescent substrate kit followed by exposure to x-ray film.

Engineering the Δ18 muCOX-2 Knock-in Mouse—Fig. 1*A* illustrates the overall process used to generate the targeting vector. The entire *Ptgs2* (COX-2) gene, including exons 1–10, was amplified by PCR using murine 129/SvJ genomic DNA (The Jackson Laboratories, stock number 000691) as a template and P1 (5′-TTGTTTTGAGCAGGGGTCTT-3′) and P2 (5′-AGCAAGAGCAGAACCATTTCA-3′) as primers. The primers were designed on the basis of sequence data from the Celera sequence data base and from the description of the original COX-2 null mouse (20). PCR was performed using the Expand long template PCR system (Roche Applied Science). The PCR product was isolated by electrophoresis on a 0.6% agarose gel and subcloned into pCR2.1 (Invitrogen) (Fig. 1*A*).

Following subcloning, the DNA fragment was verified as muCOX-2 by DNA sequencing of exons 1–10 and the adjoining intron/exon boundaries. The sequences were all identical to the COX-2 sequence in the Celera data base. The sequence encoding amino acids 595–612 of muCOX-2 was deleted using a QuikChange™ site-directed mutagenesis kit (Stratagene) and the mutagenesis oligomer primers 5′-CAGCCACCATCAATAGGCGTTCAAC-3′ and 5′-CAGCTCAGTTGAACGCCTATTGATG-3′. PCR was performed under the following conditions: denaturation at 95 °C for 1 min, 18 cycles with steps at 95 °C for 30 s, 55 °C for 1 min, 68 °C for 30 min, and 37 °C for 30 min. To insert a NotI site in the intron between exons 9 and 10, PCR was performed under the latter conditions again using a QuikChange™ site-directed mutagenesis kit with 5′-CAGCTAGTGAGCGGCCGCAAGCCTATGCTCAAC-3′ and 5′-GTTGAGCATAGGCTTGCGGCCGCTCACTAGCTG-3′ as primers.

The phosphoglycerate kinase neo poly(A) cassette flanked with two loxP sites was inserted at the NotI site in the reverse orientation. The targeting vector was sequenced to ensure that no mutation had been introduced and then linearized by XhoI digestion and electroporated into R1 ES cells (129/SvJ strain). Homologous recombinant clones were obtained from G418-resistant colonies. To screen for ES cell clones that had undergone homologous recombination correctly with the targeting vector, mouse genomic DNA was isolated from ES cells clones and screened using PCR with P7 (5′-CCACTTGTGTAGCGCCAAGT-3′) and P8 (5′-ATGTCTCTGTAGTACATAGCAC-3′) as primers (supplemental Fig. S2*A*). PCR was carried out using Ex Taq™ DNA polymerase (Takara Biochemical). Primers P7 and P8 amplified a 3.3-kbp fragment and were used to sequence the deletion site that is located in exon 10 (data not shown).

Genomic DNA (10 μg) from ES cells providing a positive response in the PCR screen was digested with BglII and separated by electrophoresis on 0.6% agarose gels. DNA was transferred to Hybond-N$^+$ (Amersham Biosciences) and hybridized with ^{32}P-labeled 5′ and 3′ probes (supplemental Fig. S2*B*). Two positive clones (WS2D2 and WS2G5) were injected into C57BL/6J blastocysts. Male chimeras were obtained, and appropriate chimeras were mated with C57BL/6J females to obtain heterozygous mice. To identify the heterozygous mice, genomic DNA was extracted from mouse tail and used for screening by PCR with P3 (5′-CAGTGACATCGATGTCATGG-3′) and P4 (5′-ACAAACACCGGAGGGAATCT-3′) as primers. PCR was carried out using Ex Taq™ DNA polymerase under the following conditions: denaturation at 94 °C for 2 min, 30 cycles with steps at 94 °C for 30 s, 55 °C for 1 min, and 68 °C for 1 min, and 68 °C 10 min. Primers P3 and P4 amplify a 524-bp native allele fragment and a 470-bp mutant allele fragment (Fig. 1*C*).

Breeding was performed to remove the neomycin gene and to put the animals into a C57BL/6J genetic background. The conditional heterozygous mice were mated with *EIIa Cre* mice having a C57BL/6J background to remove the loxP phosphoglycerate kinase neo poly(A) cassette. Genomic DNA extracted from the tails of the offspring were screened by PCR using primers P3 and P4 as described above and by sequence of intron 9 in genomic DNA to identify the removal of the loxP phosphoglycerate kinase neo poly(A) cassette. Homozygous Δ18 COX-2 knock-in mice used in the studies reported here were offspring that were derived from the breeding of heterozygous mice that had been backcrossed a minimum of six times with C57BL/6J mice. Expression of Δ18 muCOX-2 protein in mouse tissue was determined by Western blotting using antibodies to residues 595–612 of muCOX-2 and antibodies reactive with residues 583–592 of muCOX-2 as detailed above. All animal studies reported here were performed under protocols approved by University of Michigan Committee on the Use and Care of Animals.

Isolation of Mouse Dermal Fibroblasts—Mouse skin was cut from the backs of euthanized newborn mice and washed three times with ice-cold PBS containing penicillin/streptomycin. The skin was incubated in MEM containing 10% HFBS, 0.05% collagenase type A, and penicillin/streptomycin for 48 h at 4 °C. The skin was moved into a fresh 35-mm dish, broken up using a cell scraper and repeated pipetting, and incubated at 37 °C in humidified 5% CO_2 until the fibroblasts grew to 80% confluence.

Cyclooxygenase Assays—Mouse dermal fibroblast cells were cultured in DMEM medium, including 0.2% FBS for 24 h, and then treated with 1 mM aspirin for 30 min to eliminate COX-1 and residual COX-2 activities. The serum-starved cells were then washed three times with DMEM, including 0.2% FBS, to remove the aspirin and then were serum-stimulated by incubation in DMEM, including 20% FBS, to induce muCOX-2 protein. After 3 h, the medium was removed and replaced with 2 ml of MEM containing 10% FBS and 10 nmol of [1-^{14}C]arachidonic acid (~300,000 cpm) and incubated for 10 min at room temperature. Subsequently, 1 N citric acid and 10% butylated hydroxytoluene were added to stop the reaction (21), and prostaglandins were extracted from cell suspension by adding 8 ml of hexane/ethyl acetate (1:1, v/v) and centrifuged to separate the phases for 10 min at 4 °C. The organic phase was transferred into a clean glass tube maintained on ice and the extraction step repeated, and two organic phases were pooled. The organic phases were dried under N_2; the samples were reconstituted in 300 ml of ice-cold ethyl ether and applied directly to TLC plates at 4 °C. TLC plates were developed at room temperature with ethyl acetate/2,2,4-trimethylpentane/acetic acid/water (110:50:20:100, v/v). Radioactivity on the TLC plate was detected by exposure to x-ray film.

Isolation of Fibroblasts from Mouse Tails—Approximately 2-cm lengths of mouse tails were used to isolate fibroblasts using a protocol described by Salmon *et al.* (22). The mouse tail was incubated in DMEM containing 10% HFBS, 100 units/ml penicillin, and 100 μg/ml streptomycin for 1 h on ice. The tail was washed in ice-cold PBS containing penicillin/streptomycin, washed in 70% ethanol, and washed again in ice-cold PBS containing penicillin/streptomycin. The tail was diced into pieces of less than 0.5 mm^3 and digested overnight with collagenase type II (400 units/ml, 1600 units total per tail) dissolved in DMEM supplemented with 10% HFBS and penicillin/streptomycin at 37 °C in a humidified incubator with 5% CO_2. After collagenase treatment, cells were dislodged from digested tissue by repeated pipetting and filtration using a 70-μl nylon cell strainer (Falcon). The samples were centrifuged, and the collagenase solution was aspirated from the cell pellet. Cells were resuspended in DMEM with 10% HFBS and penicillin/streptomycin, split into a 60-mm dish, and incubated until the cells were confluent. Cells ($0.7–0.8 \times 10^6$ cells/dish) were seeded into 100-mm dishes with DMEM containing 10% HFBS and penicillin/streptomycin for subsequent passage. All experiments were done using cells in passages 1–6.

Expression and Degradation of COX-2 Protein in Primary Fibroblasts—Primary cells ($0.35–0.40 \times 10^6$ cells/dish) were seeded in 100-mm dishes. For serum induction of WT and Δ18 COX-2 proteins, mouse fibroblast cells were grown to about 80% confluence in 100-mm tissue culture dishes in DMEM containing 10% FBS and then serum-starved for 24 h in 8 ml of DMEM containing 0.2% FBS. The medium was changed to DMEM containing 20% FBS with or without an appropriate inhibitor such as KIF or flurbiprofen, and the cells were incu-

bated. The cells were subsequently harvested at different times, and protein levels were quantified by Western blot analyses.

To measure the rate of degradation of COX-2 protein via the ERAD pathway in primary fibroblasts, the serum-starved cells were stimulated with 20% serum containing 100 μM *S*-FBP for 4 h, and the medium was then changed to DMEM containing 20% serum, 100 μM *S*-FBP, and 50 μM cycloheximide (CHX) with or without 25 μM KIF. After a 1-h incubation, the cells were harvested at the indicated times, and cell lysate protein (15 μg/lane) was subjected to Western blotting with anti-COX-2 antibodies (αGln^{583}–Asn^{594}).

Preparation of Solubilized Microsomes from Mouse Organs for Western Blotting—Mouse organs were homogenized on ice with a Polytron homogenizer in ice-cold PBS, including 2 mM EDTA, a mixture of protease inhibitors, and 20 μM indomethacin, and then sonicated three times for 5 s. The homogenates were centrifuged at 10,000 × *g* at 4 °C for 20 min. The supernatants were centrifuged at 100,000 × *g* for 60 min to prepare a microsome fraction. Microsomes was suspended in 20 mM Tris-HCl, pH 7.4, containing 150 mM NaCl, 2 mM EDTA, 1% Nonidet P-40, 50 mM NaF, 10% glycerol, and a mixture of protease inhibitors using a glass-Teflon homogenizer and then incubated for 20 min on ice. The suspension was centrifuged at 100,000 × *g* at 4 °C for 60 min. A fraction from this supernatant (15 μg of protein) was used for Western blotting.

Isolation of Peritoneal Residential Macrophage for Western Blotting—After mice were euthanized, the peritoneal cavities were lavaged with a total of 10 ml of ice-cold PBS. Cells were harvested by centrifugation and suspended in RPMI 1640 medium with 100 units/ml penicillin and 0.10 mg/ml streptomycin, and the cells were counted. The cell were collected by centrifugation, and the cell pellet was suspended in RPMI 1640 medium supplemented with 10% heat-inactivated FBS and 100 units/ml penicillin and 0.10 mg/ml streptomycin. Cells (4.5–5.0 × 10^6) were plated on 35-mm tissue culture dishes and incubated in 2 ml of medium for 2 h. The media were changed to 2 ml of RPMI 1640 medium containing 10% HFBS, penicillin/streptomycin, 1 μg/ml LPS with or without COX inhibitor, and/or KIF for 24 h.

Isolation of Resident Peritoneal Macrophages and Assay of PGs—After the mice were euthanized, resident peritoneal macrophages were collected from untreated male mice (~12 weeks of age) by peritoneal lavage with 5 ml of ice-cold PBS (23). Cells were harvested by centrifugation and suspended in RPMI 1640 medium with 100 units/ml penicillin and 0.10 mg/ml streptomycin to count the cells. Then 2.0 × 10^5 cells were plated in 96-well plates and incubated for 30–60 min in a CO_2 incubator at which time the media were removed and fresh RPMI 1640 medium supplemented with 10% HFBS, penicillin, and streptomycin was added. After 24 h, the media were changed to 100 μl of RPMI 1640 medium containing penicillin and streptomycin with or without inhibitors, and the cells were incubated for 30 min. Then an additional 100 μl of RPMI 1640 medium containing penicillin, streptomycin, and 200 ng/ml LPS was added to each well, and the cells were incubated for different times, and the supernatants were harvested and kept at −80 °C until analyzed. PG levels in the culture medium were determined using enzyme-linked immunosorbent assay kits from Assay Designs (Ann Arbor, MI).

Measurement of Urinary PGs—Three male or female mice, either WT or Δ18 COX-2 knock-in mice, were placed in metabolic cages for 24-h urine collections. Samples were collected from a total of nine 12-week-old mice in each of the four groups. To collect the urine, three mice were placed in each metabolic cage (*i.e.* three metabolic cages were used for each group). Urine was collected each day for 3 days, and then randomly five samples from each group were analyzed; thus, two samples of the five were from the same cage but were collected on different days. Urine was centrifuged to remove any precipitated matter. The supernatants were kept −80 °C until analyses. The urinary metabolite of prostaglandin E_2 was measured using a liquid chromatography/tandem mass spectrometric method described previously (24).

Implantation of Telemeters and Monitoring Body Temperature—Radiofrequency telemeters (model ETA10-F20, Data Sciences International, St. Paul, MN) were surgically implanted in the peritoneal cavity of male mice (16–20 weeks old) under anesthesia, as described previously (25, 26). At least 21–28 days were allowed for recovery from surgery before the experiments began. Temperature data were acquired every 10 min as detailed previously (26). Circadian temperature variation was assessed by monitoring the body temperature of undisturbed animals at 10-min intervals over two consecutive 24-h periods. These 48-h data were averaged and represented a single 24-h period. Base-line body temperature was defined as the average body temperature for the 60 min before any treatment. Mice were subsequently injected intraperitoneally with pyrogen-free saline, and body temperature was recorded for 24 h. The same mice were then injected intraperitoneally with 10 μg of LPS (*E. coli* O111:B4, Sigma) dissolved in pyrogen-free saline, and body temperature was measured for another 24 h. Each mouse administered pyrogen-free saline served as its own control for subsequent LPS exposure. Treatments were conducted at 9:00 a.m. to reduce the effects of circadian variation on the results.

For either WT ($n = 6$) or Δ18 COX-2 mice ($n = 5$), statistical comparisons between the mean hourly body temperature data following saline and LPS treatment were conducted using a two-way analysis of variance with Bonferroni post hoc test. For comparisons between WT and Δ18 COX-2 mice treated with LPS, differences between pyrogen-free saline-treated body temperature and matched LPS-treated body temperature measurements were calculated (denoted ΔT_b), and then sequential 10 min ΔT_b values were averaged hourly to calculate mean hourly ΔT_b. Matched hourly ΔT_b data were compared by Student's *t* test. $p \leq 0.05$ was considered statistically significant.

Cardiovascular Parameters of Δ18 COX-2 Mice—Cardiovascular parameters were measured by the University of Michigan Medical School Integrative Genomics using nine, 12-week-old mice in each group (27). Ejection fractions were determined with echocardiograms (27, 28). Values are reported as mean ± S.D.

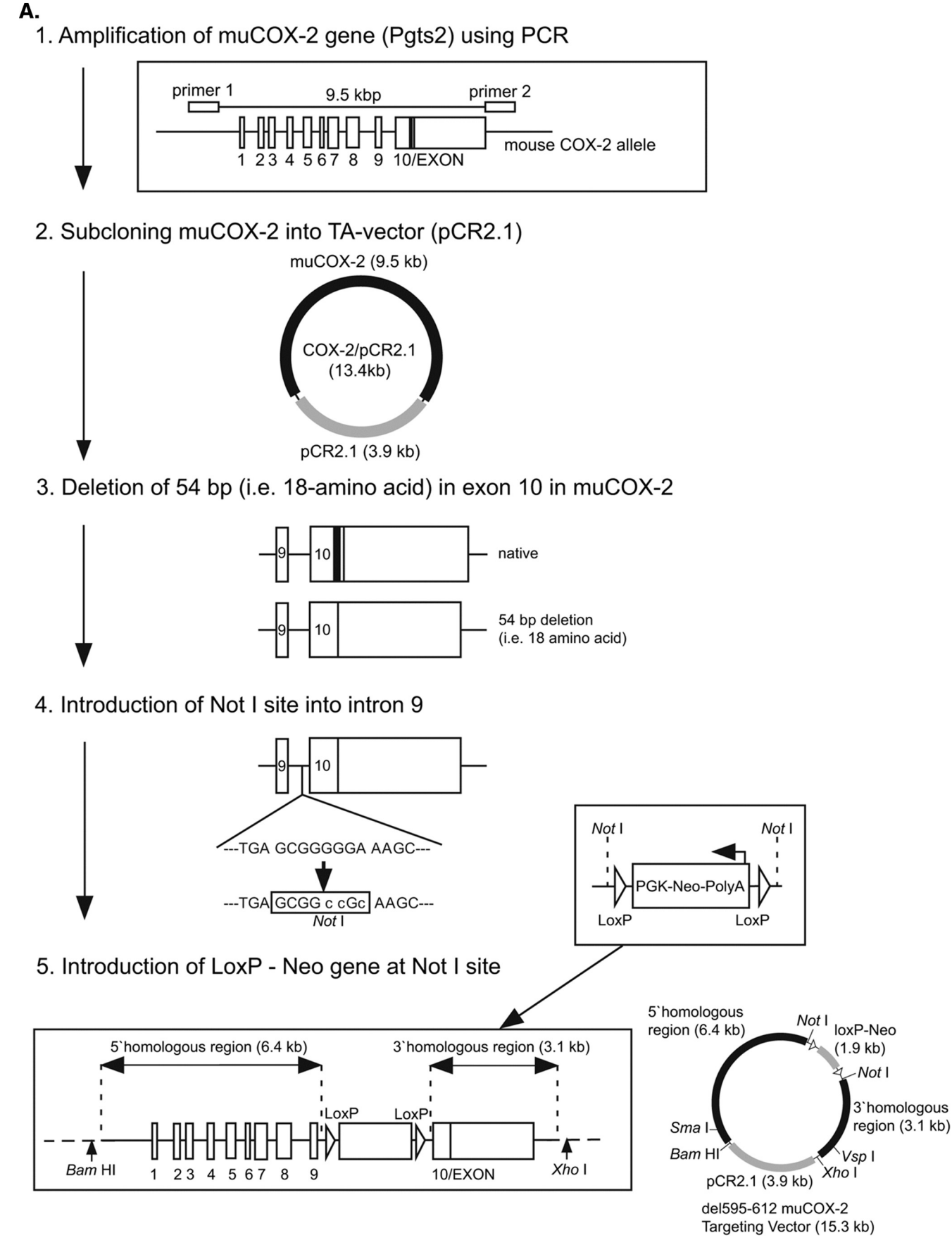
A.
1. Amplification of muCOX-2 gene (Pgts2) using PCR
primer 1
9.5 kbp
primer 2
mouse COX-2 allele
1 2 3 4 5 6 7 8 9 10/EXON
2. Subcloning muCOX-2 into TA-vector (pCR2.1)
muCOX-2 (9.5 kb)
COX-2/pCR2.1
(13.4kb)
pCR2.1 (3.9 kb)
3. Deletion of 54 bp (i.e. 18-amino acid) in exon 10 in muCOX-2
9
10
native
54 bp deletion
(i.e. 18 amino acid)
4. Introduction of Not I site into intron 9
---TGA GCGGGGGA AAGC---
---TGA GCGG c cGc AAGC---
Not I
Not I
Not I
PGK-Neo-PolyA
LoxP
LoxP
5. Introduction of LoxP - Neo gene at Not I site
5`homologous region (6.4 kb)
3`homologous region (3.1 kb)
LoxP
LoxP
Bam HI
1 2 3 4 5 6 7 8 9
10/EXON
Xho I
5`homologous
region (6.4 kb)
Not I
loxP-Neo
(1.9 kb)
Not I
3`homologous
region (3.1 kb)
Sma I
Bam HI
Vsp I
Xho I
pCR2.1 (3.9 kb)
del595-612 muCOX-2
Targeting Vector (15.3 kb)

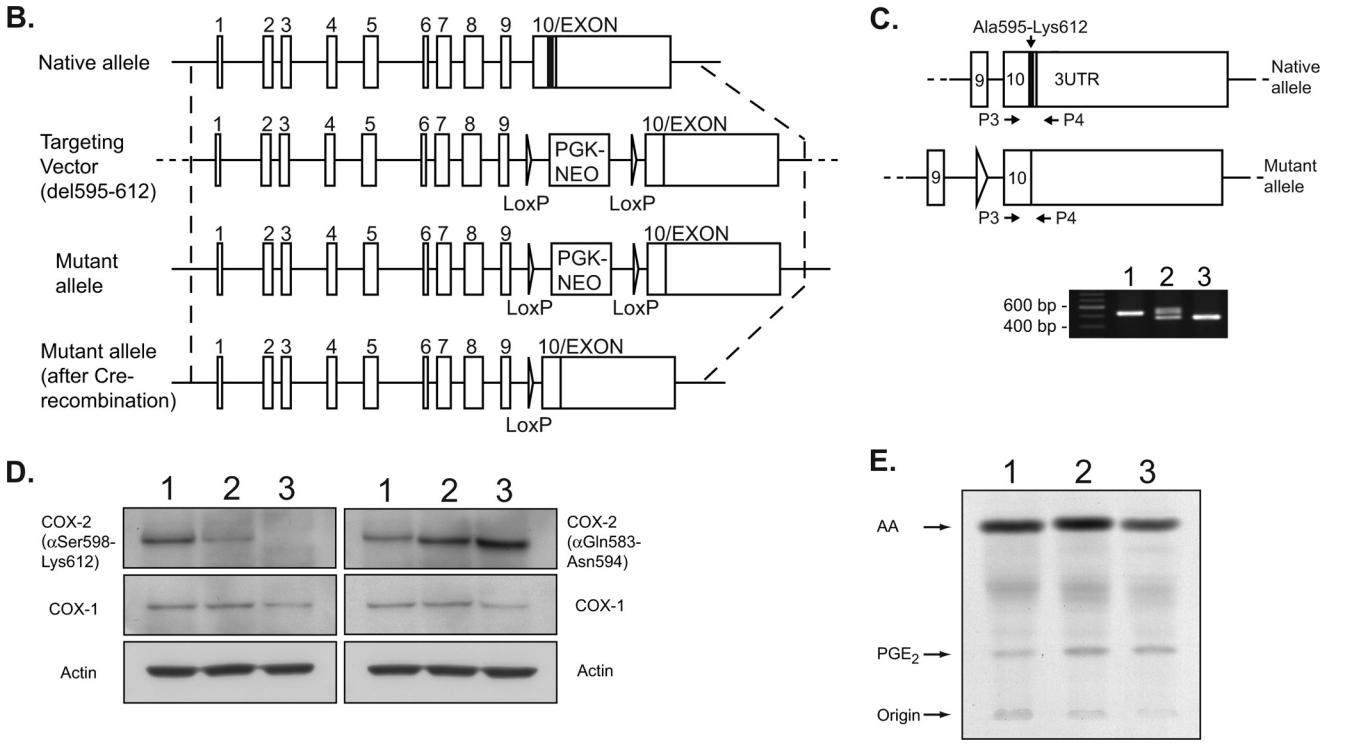

FIGURE 1—*continued*

RESULTS

Preparation of Δ18 COX-2 Mouse—Previous studies have indicated that human (hu) COX-2 expressed heterologously in HEK293 cells undergoes *N*-glycosylation of Asn^{594} as a prelude to entry into the ERAD pathway. Additional studies with mutants of murine (mu) COX-2 also expressed in HEK293 cells corroborate these results (supplemental Fig. S1).

To determine the importance in COX-2 biology of the 27-amino acid instability motif (27-IM) located near the C terminus of the protein, we prepared a knock-in (Δ18 COX-2) mouse lacking 18 residues (595–612) of the 27-IM. The Δ18 COX-2 protein is catalytically indistinguishable from native COX-2, but unlike wild type (WT) COX-2, it is unable to undergo *N*-glycosylation of Asn^{594} and degradation via the ERAD pathway (17). Fig. 1*A* illustrates how the targeting vector was constructed. To generate the Δ18 COX-2 knock-in mice, homologous recombination in ES cells was used to create the mutant allele (Fig. 1*B*), and selected recombinant ES cells (supplemental Fig. S2, *A* and *B*) were used for the generation of the Δ18 COX-2 knock-in mice. To remove the Lox P phosphoglycerate kinase neo poly(A) cassette, the knock-in mice were mated with Cre recombinase expressing *EIIa Cre* transgenic mice, and the genotypes of the mice were identified by PCR (Fig. 1*C*). PCR fragments of appropriate sizes (524 and/or 470 bp) were observed for DNA isolated from mice expressing only WT COX-2, only Δ18 COX-2, or both WT and Δ18 COX-2.

To determine the level of COX-2 protein expression, we cultured dermal fibroblasts from newborn WT, Δ18 COX-2, and heterozygous mice. The cultured cells were subjected to serum starvation, which typically reduces the levels of native COX-2 in normal fibroblasts to near zero and then, as shown in Fig. 1*D*, the cells were stimulated with serum to induce COX-2 gene transcription. The αSer^{598}–Lys^{612} antibody cannot recognize Δ18 COX-2 protein, whereas the αGln^{583}–Asn^{594} antibody can recognize both WT COX-2 and Δ18 COX-2 protein. As expected, there is no COX-2 immunoreactivity in cell

FIGURE 1. **Preparation and characterization of the Δ18 COX-2 knock-in mouse.** *A,* preparation of the targeting vector. Experimental details are provided under "Experimental Procedures." *B,* diagram comparing wild type (WT) COX-2 and *del*595–612 PGHS-2 (Δ18) COX-2 mutant alleles. *C,* PCR analysis of DNA from WT COX-2 (*lane 1*), WT/Δ18 heterozygous COX-2 (*lane 2*), and homozygous Δ18 COX-2 (*lane 3*) mice. The *left lane* contains Invitrogen markers differing in length by 100 bp. DNA was isolated from tail snips from animals after removal of the LoxP site from the mutated (*i.e.* Δ18 COX-2) gene and subjected to PCR analysis using primers P3 and P4 as detailed under "Experimental Procedures." Shown at the *top* of the panel are intron/exon diagrams illustrating the location of the 18-amino acid (*i.e.* 54 bp) deletion in Exon 10 (*black bar* in native allele diagram), the LoxP site in the intron (*sidewise arrow* in mutant allele diagram), and the expected PCR fragment sizes based on the locations of primers P3 and P4. *UTR,* untranslated region. *D,* COX-2 protein expression in dermal fibroblasts from WT, heterozygous, and Δ18 COX-2 mice. Dermal fibroblasts were isolated from the skin of newborn WT (*lane 1*), WT/Δ18 heterozygous (*lane 2*), or Δ18 COX-2 (*lane 3*) mice and grown to about 60% confluence in MEM containing 10% FBS as described under "Experimental Procedures." The cells were serum-starved for 24 h in MEM containing 0.2% FBS. Serum-starved dermal fibroblasts were then treated with MEM containing 20% FBS for 3 h. The cells were harvested, and cell lysate protein (15 μg/lane) was subjected to Western blotting using antibodies to actin, COX-1, or COX-2. Two different anti-COX-2 anti-peptide antibodies were used directed against either Ser^{598}–Lys^{612} or Gln^{583}–Asn^{594}. *E,* cyclooxygenase activity of dermal fibroblasts from WT, heterozygous, and Δ18 COX-2 mice. Dermal fibroblasts were cultured and serum-starved for 24 h as described in *D* and then treated with 1 mM aspirin for 30 min to eliminate COX-1 and residual COX-2 activities. The cells were then washed to remove the aspirin and incubated in MEM containing 20% FBS for 3 h. Finally, the cells were washed with MEM without serum and then incubated with 5 μM [1-^{14}C]arachidonic acid in MEM for 10 min at room temperature. Lipid products were extracted from the medium and separated by TLC as described under "Experimental Procedures." Based on scintillation counting, the relative conversion of arachidonic acid to total products was 2.8, 4.3, and 5.8% for cells from WT (*lane 1*), WT/Δ18 heterozygous (*lane 2*), and Δ18 COX-2 (*lane 3*) mice, respectively.

TABLE 1

Cardiovascular parameters of WT and Δ18 COX-2 mice

Cardiovascular parameters were measured using nine, 12-week-old mice in each group except for the Δ18 COX-2 female group where there were eight animals. Details are provided under "Experimental Procedures." The abbreviations used are as follows: bpm, beats/min; bp, blood pressure; EF%, ejection fraction. Mean ± S.D.

Animal	Body weight	Heart rate	Systolic bp	EF
	g	*bpm*	*mm Hg*	*%*
WT, male	22 ± 1.2	760 ± 18	103 ± 14	51 ± 6.5
Δ18 COX-2, male	21 ± 1.0	762 ± 23	96 ± 8.2	55 ± 3.5
WT, female	18 ± 1.0	785 ± 11	125 ± 8.8	60 ± 2.0
Δ18 COX-2, female	18 ± 1.0	762 ± 24	103 ± 7.6	54 ± 7.6

extracts from Δ18 COX-2 mice in Western blots performed with the αSer^{598}–Lys^{612} antibody. Western blots performed with the αGln^{583}–Asn^{594} antibody indicate that Δ18 COX-2 levels are higher than WT COX-2 levels in the serum-stimulated fibroblasts.

As shown in Fig. 1*E*, serum-stimulated dermal fibroblasts from WT COX-2, Δ18 COX-2, and heterozygous mice retain COX-2 catalytic activity in approximate proportion to the amount of immunoreactive COX-2 protein and form the same products from arachidonic acid (*e.g.* PGE_2). These results are consistent with previous *in vitro* data showing that WT COX-2 and Δ18 COX-2 are kinetically indistinguishable (17).

The data in Fig. 1 indicate that engineered Δ18 COX-2 mice exhibit homozygous expression of a functional Δ18 COX-2 of the appropriate size. Δ18 COX-2 knock-in mice were backcrossed at least six generations into the C57BL/6J mouse strain prior to performing the experiments described below.

Phenotyping of Δ18 COX-2 Knock-in Mice—Δ18 COX-2 mice have the same physical appearance as WT mice. The animals undergo normal growth; female Δ18 COX-2 mice have normal litter sizes (supplemental Table S1), and no renal glomerular defects were observed by light microscopy (supplemental Fig. S3).[3] Thus, Δ18 COX-2 mice have a very different phenotype than COX-2 null mice (20).

Cardiovascular parameters for WT and Δ18 COX-2 male and female mice are summarized in Table 1. No statistically significant differences were observed in heart rates, blood pressure, or cardiac output (*i.e.* ejection fraction) with age- and sex-matched mice. We did observe that the mutant mice showed smaller variations in blood pressure. We were somewhat surprised by the lack of any obvious cardiovascular phenotype because we had expected Δ18 COX-2 mice to overexpress COX-2 and to overproduce vascular PGI_2 (29), which, if uncompensated, would have led to changes in cardiovascular performance (*e.g.* decreased blood pressure).

The levels of the urinary metabolite of PGE_2 were significantly higher (~50%) in 12-week-old male Δ18 knock-in mice than in male WT control mice (Fig. 2). Approximately half of

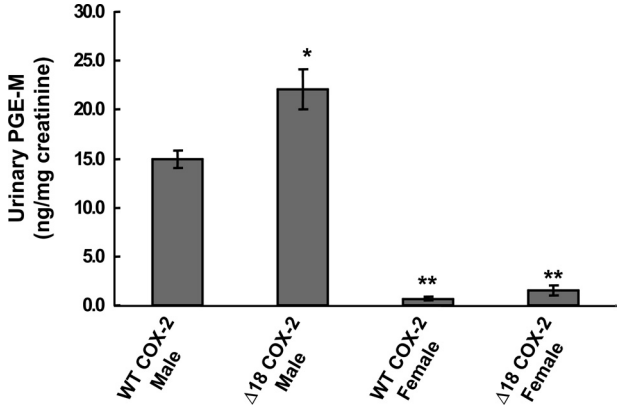

FIGURE 2. **Urinary PGE_2 metabolites from adult male WT or Δ18 COX-2 mice.** Analyses of urinary PGE_2 metabolites (*PGE-M*) were performed as described in detail under "Experimental Procedures" using urine collected from 12-week-old mice. Data are means ± S.E. * indicates a difference from the value for the male WT; ** indicates a difference from the value for male WT but no difference between the values for the WT and Δ18 female mice ($p < 0.05$).

urinary PGE_2 metabolites are formed via COX-2 in WT mice (30), so a 50% increase in the total PGE_2 metabolites in the knock-in mice may represent an approximate doubling of COX-2-derived PGE_2 formation. This would be consistent with overexpression of COX-2. It is not known why the levels of urinary PG metabolites are so much higher in the male than the female mice in C57BL/6J mice. This is clearly dependent on the genetic background of the mice because females have higher levels of PGE_2 urinary metabolites than the males in the DBA/1 mouse background (31).

COX-2 Expression in Tail Fibroblasts from WT Versus Δ18 COX-2 Knock-in Mice—Primary fibroblasts prepared from the tails of WT and Δ18 COX-2 mice were used to evaluate the importance of residues 595–612 of COX-2 in the degradation of the protein via the ERAD pathway (Fig. 3, *A*–*C*). In these experiments serum-starved cells were treated with 20% serum to induce COX-2 protein expression. The experiments depicted in Fig. 3, *A* and *B*, were performed in the presence or absence of the following: (*a*) kifunensine (KIF), which blocks processing of *N*-glycosylated carbohydrate and retards entry of *N*-glycosylated protein into the ERAD pathway, and/or (*b*) the nonspecific COX inhibitor *S*-flurbiprofen, which prevents substrate turnover. No inhibitor of translation was included in the experiments shown in Fig. 3, *A* and *B*. In the absence of KIF or flurbiprofen, WT and Δ18 COX-2 protein undergo degradation in a temporally similar manner, although the level of COX-2 expression is much higher with Δ18 COX-2. The disappearance of immunoreactive COX-2 is completely blocked by flurbiprofen in fibroblasts from Δ18 COX-2 but not WT COX-2 mice; flurbiprofen slows but does not prevent the disappearance of WT COX-2. In the presence of KIF alone or KIF plus *S*-flurbiprofen, two immunoreactive COX-2 bands are present in fibroblasts from WT but not Δ18 COX-2 mice. The upper band results primarily from *N*-glycosylation of Asn^{594} in WT COX-2. Δ18 COX-2 is missing the consensus sequence for *N*-glycosylation of Asn^{594} and cannot be glycosylated on this residue. KIF by itself does not stabilize Δ18 COX-2.

The experiment shown in Fig. 3*C* was performed in the presence of both an inhibitor of protein synthesis cycloheximide

[3] We have noted two morphologic differences in Δ18 COX-2 mice, but we have not explored either in sufficient detail to establish significance as follows: (*a*) gastrointestinal abnormalities (apparent paralytic ileus) in response to fasting and refeeding, and (*b*) enlarged spleens in some older knock-in mice. In the febrile response experiments, we noted that after the surgery to implant the telemeters, four of the original nine Δ18 COX-2 mice exhibited a bowel obstruction (ileus) within the week. In the WT mice only one of eight mice exhibited this phenotype. Although not statistically significant, we suspect that prostaglandins overproduced in the peritoneal cavity in Δ18 COX-2 mice are associated with ileus.

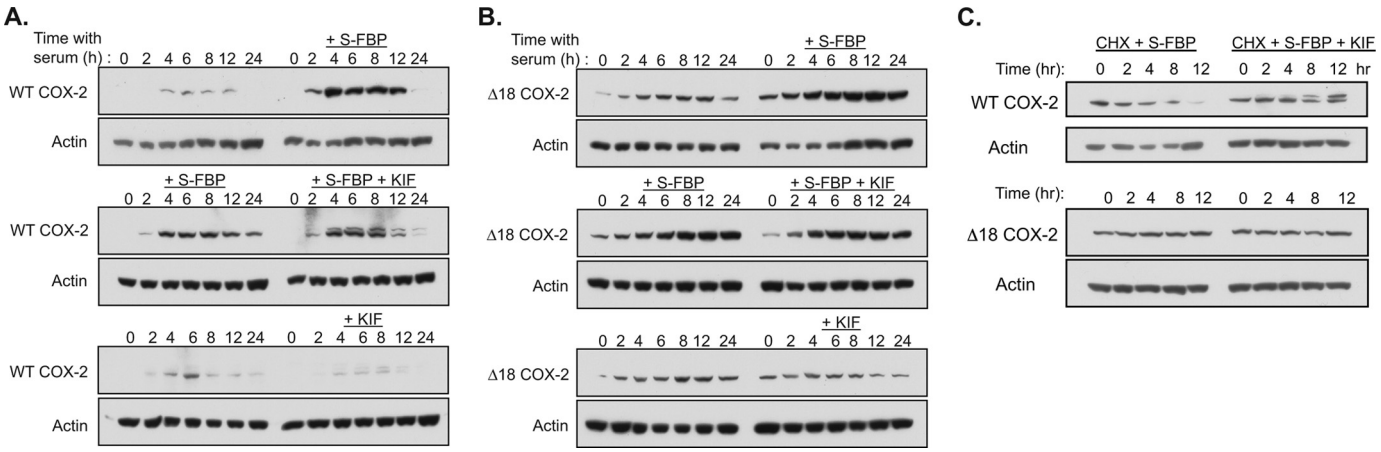

FIGURE 3. **COX-2 protein expression and degradation in tail fibroblasts from WT and Δ18 COX-2 mice.** Fibroblasts were isolated from the tails of 1–3 male mice as detailed under "Experimental Procedures" for one mouse. *A,* WT mice; *B,* Δ18 COX-2 mice; *C,* both WT and Δ18 COX-2 mice. The cells were grown and serum-starved as described under "Experimental Procedures" and the legend to Fig. 1. Serum-starved tail fibroblasts were stimulated with DMEM containing 20% FBS for the indicated times in media containing no additions, *S*-FBP (100 μM), *S*-FBP plus KIF (25 μM), or KIF alone. *C,* cells were stimulated with 20% serum containing 100 μM *S*-FBP for 4 h, and then the medium was changed to DMEM containing 20% serum, 100 μM *S*-FBP. and 50 μM CHX with or without 25 μM KIF. After a further 1-h incubation, the cells were harvested at the indicated times, and cell lysate protein (15 μg/lane) was subjected to Western blotting using antibodies to actin or COX-2 (αGln^{583}–Asn^{594}). The experiments were performed at least twice with similar results.

(CHX) and FBP, which inhibits degradation via the suicide pathway. It can be seen that WT COX-2 is degraded, and degradation is inhibited by KIF. However, Δ18 COX-2 is not degraded under these conditions. The data in Fig. 3, *A–C,* indicate that Δ18 COX-2 protein can be degraded via the substrate-dependent degradation pathway but not the ERAD pathway. The lack of a functional 27-IM caused by deletion of residues 595–612 stabilizes Δ18 COX-2 in cells from the knock-in mouse where Δ18 COX-2 is under the control of the WT muCOX-2 promoter. These results obtained with mouse tail fibroblasts are consistent with those obtained *in vitro* in HEK293 cells heterologously expressing WT or mutant forms of human COX-2 (18).

COX-2 Expression in Brain, Kidney, Spleen, and Heart—Western transfer blotting was performed on extracts of several tissues from WT and Δ18 COX-2 mice to assess the relative importance of the ERAD pathway in COX-2 degradation (supplemental Fig. S3 and Fig. 4). The basal levels of immunoreactive COX-2 are lower in brain tissue from WT COX-2 mice than Δ18 COX-2 mice suggesting that the ERAD pathway is important in COX-2 degradation in brain. In contrast, the basal levels of immunoreactive COX-2 are similar in heart (supplemental Fig. S4), kidney, and spleen from WT COX-2 and Δ18 COX-2 mice.

The two panels labeled *Brain* in Fig. 4 represent the same Western blot with different exposure times; the lower *Brain panel* is included to permit comparisons of the levels of WT and Δ18 COX-2 in brain, kidney, and spleen. The basal levels of WT COX-2 are low in brain, intermediate in kidney, and relatively high in spleen. LPS treatment of normal mice leads to increased expression of WT COX-2 in brain and spleen but not kidney. Treatment of animals with ibuprofen at analgesic doses (32), which would be expected to interfere with substrate-dependent degradation of COX-2, increased the levels of WT COX-2 in brain from WT animals, and the effect was observed with and without (*i.e.*"0" time point) LPS. In contrast, ibuprofen treatment had no obvious effect on the levels of WT COX-2 in kidney or spleen from either LPS-treated or untreated animals. The levels of immunoreactive Δ18 COX-2 in brain, kidney, and spleen were unchanged by LPS treatment. Overall, the results shown in Fig. 4 suggest that both the ERAD and substrate turnover-dependent pathways are important in COX-2 degradation in brain. It is unclear what pathways are involved in COX-2 protein degradation in kidney and spleen. Compensatory mechanisms involving enhanced expression and/or decreased degradation of COX-2 must exist in kidney and spleen to maintain COX-2 levels constant in these tissues (*e.g.* when the ERAD pathway is disrupted in the Δ18 COX-2 mice).

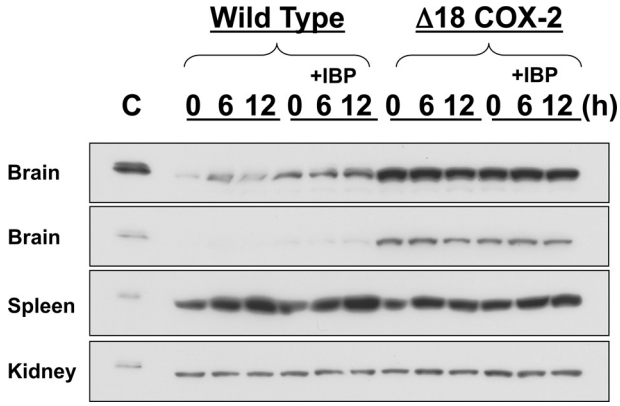

FIGURE 4. **Expression of COX-2 in tissues from WT and Δ18 COX-2 mice treated with endotoxin with or without ibuprofen.** Microsomal protein was prepared from whole brain, whole kidney, and whole spleen obtained from 12-week-old male WT or Δ18 COX-2 mice. Animals were subjected to an intraperitoneal injection with LPS (10 μg) and were euthanized, and tissues were taken at the indicated times following the LPS injection. Half of the animals received ibuprofen (+*IBP*) in their drinking water (0.2 mg/ml) beginning 2 days prior to the LPS treatment and also received an intraperitoneal injection of ibuprofen (40 mg/kg) in saline 30 min prior to the LPS injection. *C,* control WT muCOX-2 (0.05 μg); the adjacent lane contained molecular weight standards (not visible). The same amounts of microsomal protein were applied in each lane. The *two Brain panels* represent different exposure times for the same Western blot. The *columns* in each of the panels represent tissue from the same mouse (*i.e.* one mouse was used for each time point). Anti-COX-2 (Novus Biologicals) antibody was used for Western blotting.

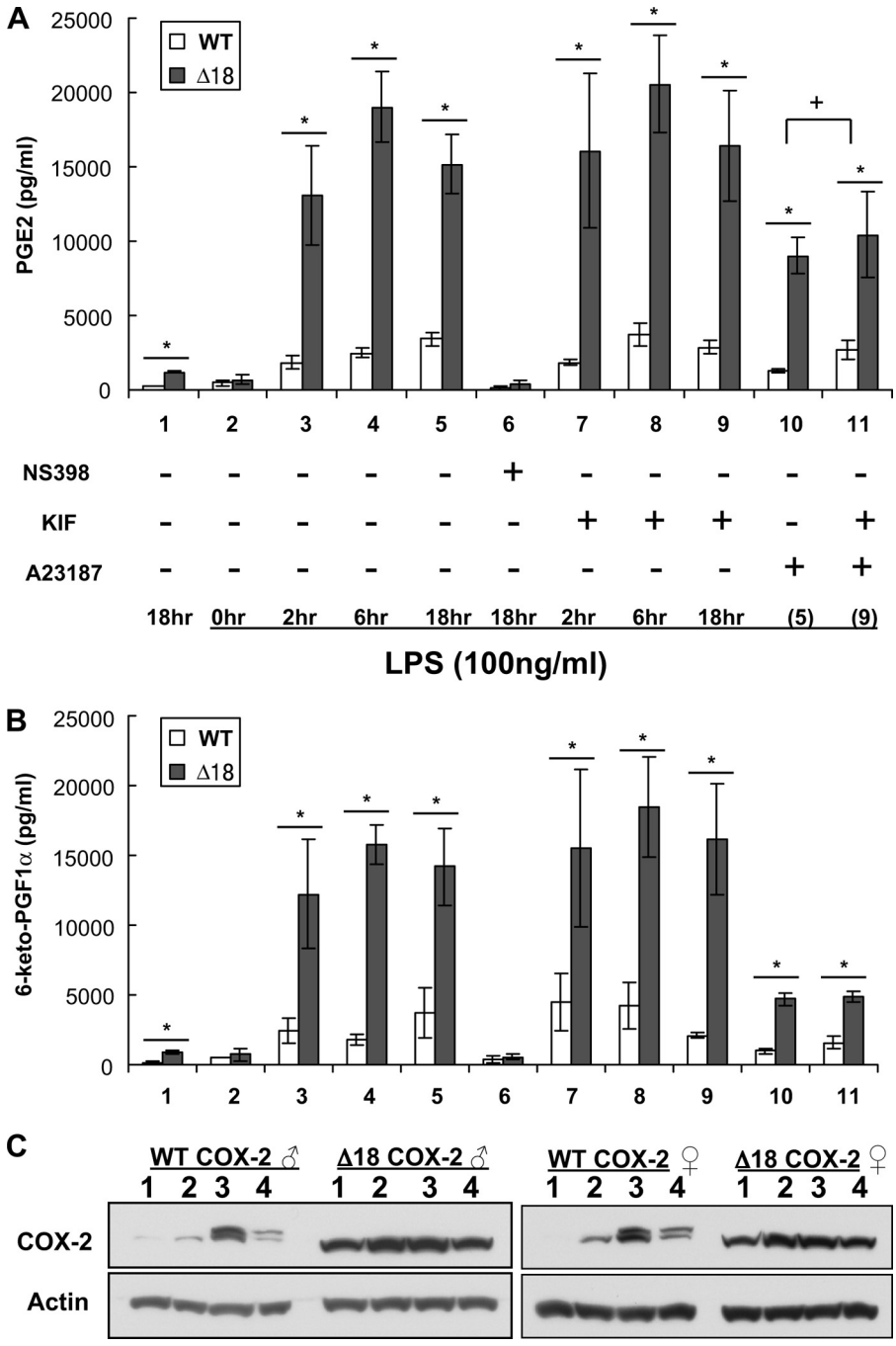

FIGURE 5. **Prostanoid formation and expression of COX-2 in peritoneal macrophages from WT and Δ18 COX-2 mice.** Resident peritoneal macrophages were isolated from 12-week-old adult male mice as described under "Experimental Procedures." After 24 h, PGE_2 (*A*) and 6-keto-$PGF_{1\alpha}$ levels (*B*) in the media were measured after the following treatments: *lane 1,* 18 h without LPS; *lane 2,* 0 h with LPS; *lane 3,* 2 h with LPS; *lane 4,* 6 h with LPS; *lane 5,* 18 h with LPS; *lane 6,* 18 h with LPS and NS398; *lane 7,* 2 h with LPS and KIF; *lane 8,* 6 h with LPS and KIF; *lane 9,* 18 h with LPS and KIF; *lane 10,* cells were harvested after 18 h with LPS (as in *lane 5*), and new medium containing with A23187 was added and the sample incubated for 30 min before measuring PGs; and *lane 11,* cells were harvested after 18 h with LPS and KIF (as in *lane 9*), and new medium containing with A23187 was added and the sample incubated for 30 min before measuring PGs. *Error bars,* ± S.D. *, $p < 0.05$ for comparison between WT and Δ18 COX-2 mice. Statistical analysis was performed by Student's *t* test. *C,* resident peritoneal macrophages were isolated from male and female mice as described under "Experimental Procedures" and treated for 24 h with the following: *lane 1,* LPS; *lane 2,* LPS plus *S*-flurbiprofen; *lane 3,* LPS plus *S*-flurbiprofen plus KIF; or *lane 4,* LPS plus KIF. The cells were homogenized and the extracts subjected to Western transfer blotting for COX-2 and actin as indicated in the legend to Fig. 1.

Prostaglandin Formation by LPS-treated Peritoneal Macrophages—When peritoneal macrophages isolated from WT and Δ18 COX-2 mice were treated with LPS, cells from the Δ18 COX-2 mice produced considerably more PGE_2 and PGI_2 (measured as 6-keto-$PGF_{1\alpha}$) than cells from WT mice (Fig. 5, *A* and *B*). Again, this is consistent with the ERAD pathway playing an important role in COX-2 degradation in macrophages. Macrophages treated with KIF to slow degradation of COX-2 by interfering with ERAD degradation produced slightly higher amounts of PGE_2 in response to the Ca^{2+} ionophore A23187 (Fig. 5*A, lanes 10* and *11*).

It can be seen that the levels of immunoreactive COX-2 higher at base line in macrophages from both male and female Δ18 COX-2 mice are relatively unaffected by LPS, flurbiprofen, and/or KIF (Fig. 5*C*). This is similar to what is observed with brain, kidney, and spleen from Δ18 COX-2 mice (Fig. 4). In contrast, COX-2 levels in macrophages from WT mice increase in a predictable manner following treatments with LPS, LPS and flurbiprofen, and LPS plus KIF (18) (Fig. 5*C*); the lower band of the protein doublet seen when KIF is included is COX-2 with three asparagine residues glycosylated, whereas glycosylation at a fourth asparagine, primarily Asn^{594}, results in formation of the band with slower electrophoretic mobility (18).

Febrile Response—COX-2 is known to be important in thermoregulatory responses to inflammatory insults such as infection (33, 34). Therefore, experiments were conducted to investigate the impact of the Δ18-modified COX-2 on thermoregulatory physiology both at rest and under inflammatory stress, induced by intraperitoneal injection of LPS. As depicted in Fig. 6*A*, both WT and Δ18 COX-2 mice exhibited normal basal body temperatures and intact circadian variability. Although both WT and Δ18 COX-2 mice became febrile following LPS administration (Fig. 6, *B* and *C*), significant differences were noted in these responses. In the WT animals, core body temperature was significantly greater after LPS injection compared with saline administration beginning ~5 h after the injections and persisting for 3 h (Fig. 6*B*). In contrast, sig-

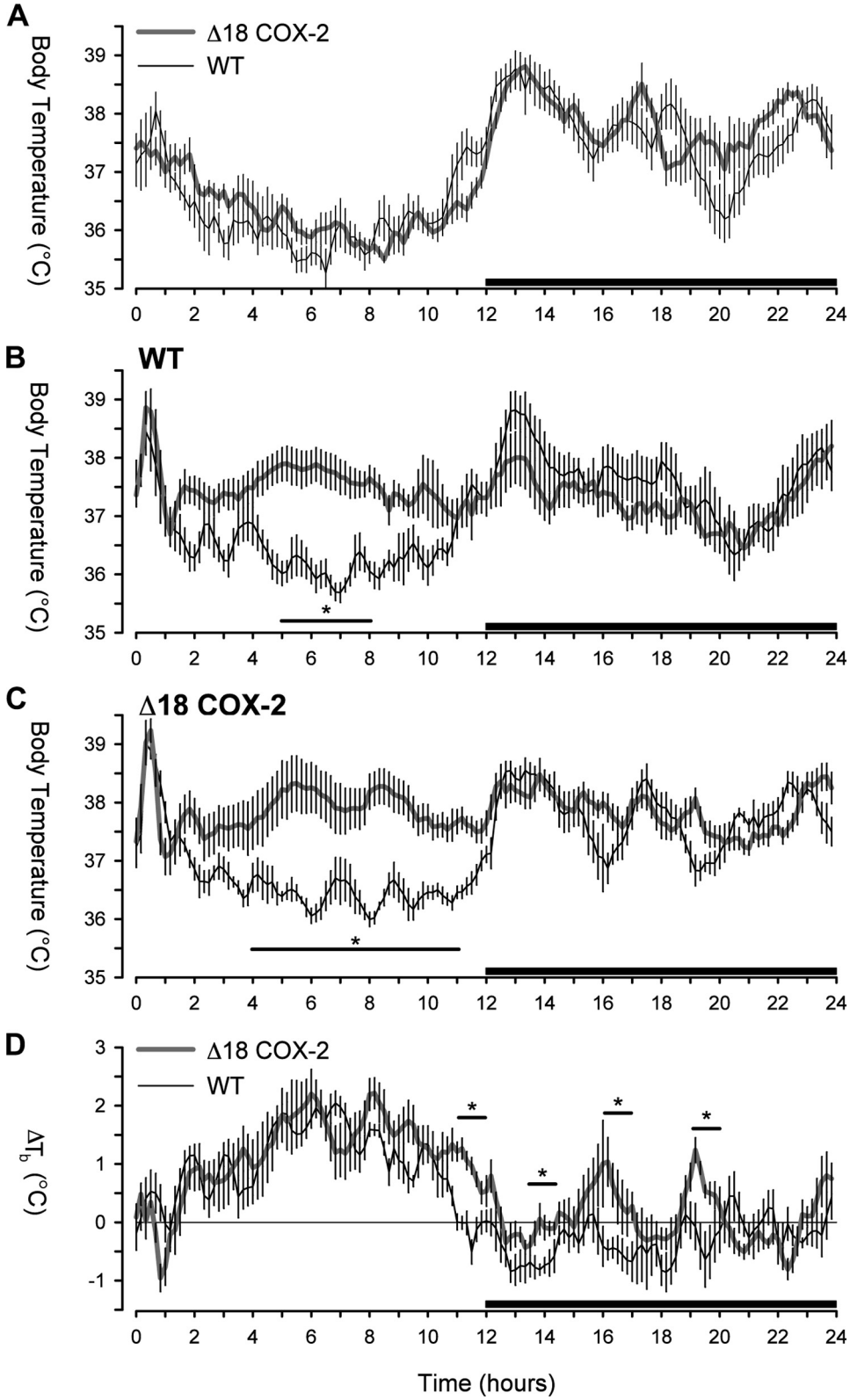

FIGURE 6. **Endotoxin-induced febrile response in adult male WT and Δ18 COX-2 mice.** WT and Δ18 COX-2 mice that had had telemeters implanted were treated as detailed under "Experimental Procedures." *A,* body temperatures of untreated mice demonstrate normal circadian variability in WT (*thin line*) and Δ18 COX-2 mice (*thick line*); *B,* WT mice were injected with pyrogen-free saline (*thin line*) or LPS (*thick line*, 10 μg) at time 0. The *horizontal line* with *asterisk* denotes statistically significant differences in mean hourly temperature ($p < 0.01$). *C,* Δ18 COX-2 mice were injected with pyrogen-free saline (*thin line*) or LPS (*thick line*, 10 μg) at time 0. The *horizontal bar* with *asterisk* denotes statistically significant differences in mean hourly temperature ($p < 0.01$). Body temperature measurements shown in the figure represent mean and S.E. of values obtained from six WT mice and five Δ18 COX-2 mice. *D,* comparison of the mean hourly difference in body temperature (ΔT_b) between pyrogen-free saline and LPS treatment for WT (*thin line*) and Δ18 COX-2 mice (*thick line*). Mean hourly ΔT_b values were calculated as described under "Experimental Procedures." *Horizontal black lines* with *asterisks* denote hour periods during which statistically significant differences ($p < 0.05$) were revealed between WT and corresponding Δ18 COX-2 mice. *Dark bars* on the *x* axis denote the dark period of the light/dark cycle.

nificant differences in core body temperature between LPS and saline administration became evident ~4 h after injection in the Δ18 COX-2 mice and remained statistically significant for 7 h (Fig. 6*C*). Increases in body temperature induced by LPS over saline alone were significantly more pronounced in the Δ18 COX-2 mice *versus* the WT animals for as long as 20 h after the treatments were administered (Fig. 6*D*).[3]

DISCUSSION

In this study, we successfully generated Δ18 COX-2 knock-in mice and established that the Δ18 COX-2 protein has COX activity and that Δ18 COX-2 is more stable than the WT enzyme in at least some tissues (*i.e.* brain). In combination with other *in vitro* studies of the mechanism of COX-2 protein degradation (17, 18), our results indicate that the ERAD pathway participates in COX-2 protein degradation *in vivo*. Substrate-dependent loss of WT COX-2 is inhibited by flurbiprofen in murine 3T3 fibroblasts and in HEK293 cells heterologously expressing human COX-2 (18). Similarly, we find that flurbiprofen leads to accumulation of immunoreactive COX-2 protein in both cultured fibroblasts and macrophages from WT and Δ18 COX-2 mice. WT COX-2 also accumulates in brain tissue from normal mice treated with ibuprofen, a nonsteroidal anti-inflammatory drug closely related to flurbiprofen. These data suggest that substrate-dependent loss of COX-2 occurs *in vivo*. Like flurbiprofen, KIF treatment of cultured cells from WT and Δ18 COX-2 mice also causes the accumulation of COX-2 protein even in the presence of flurbiprofen.

The manner in which the ERAD and substrate turnover-dependent degradation pathways are related is unclear. They may be parallel noninteracting pathways of degradation. However, it is also possible that there is an additional level of complexity such that *N*-glycosylation at Asn^{594} somehow interferes with the ability of the enzyme to encounter substrate and undergo substrate-dependent degradation.

Our most unexpected finding was the lack of accumulation of Δ18 COX-2 above levels seen with WT COX-2 in several tissues, including kidney, heart, and spleen. This implies that there are previously unappreciated processes involved in maintaining COX-2 protein levels that presumably involve cross-talk between pathways involved in COX-2 synthesis and degradation. These changes could involve decreased rates of transcription and/or translation (6, 7, 16). We did not measure COX-2 mRNA levels in our samples. There are examples in the literature suggesting that there is cross-talk between PG production and COX-2 gene expression (6, 7).

When Δ18 COX-2 knock-in mice are subjected to a physiological stress, specifically treatment with bacterial endotoxin, the febrile response is enhanced, and Δ18 COX-2 accumulates in brain. Similarly, resident peritoneal macrophages prepared from Δ18 COX-2 mice produce more PGs than cells from WT COX-2 mice upon endotoxin treatment. Again, this is consistent with overexpression of Δ18 COX-2 in cells from knock-in mice.

COX-2-derived PGE_2 is a central mediator in the febrile response to infection and inflammation (33, 34), but evidence suggests that eicosanoids do not control normal, nonfebrile thermoregulation (35). Our results support this paradigm, as no differences were observed in either basal body temperature or circadian temperature variation between WT and Δ18 COX-2 mice. Notably, however, mice harboring the Δ18 COX-2 variant exhibited aberrant thermoregulation in the face of systemic inflammation. We found a prolonged febrile response in Δ18 COX-2 mice after intraperitoneal LPS administration compared with WT COX-2 mice, and this correlated with higher levels of Δ18 COX-2 in the brains of the transgenic animals relative to the levels of normal COX-2 in the WT mouse brains. These data support a role for COX-2 in the febrile response to LPS and suggest that the ERAD pathway for COX-2 degradation plays a role in controlling the amplitude and duration of the febrile response.

The Δ18 COX-2 knock-in mouse has what appears to be a largely normal phenotype. Nonetheless, there is about a 50% increase in the level of the major PGE_2 urinary metabolite in male Δ18 COX-2 knock-in mice. This is consistent with an increase in the level of COX-2 protein and activity in Δ18 COX-2 knock-in mice. Mice 3–6 months of age were used in these studies, and it is not known if the knock-in mice would display any abnormalities with age. It is known that cancer patients and individuals with rheumatoid arthritis have elevated levels of PGE_2 production. Δ18 COX-2 mice that chronically overproduce prostaglandins via COX-2 may be useful in studying the development of chronic inflammation and colon cancer.

Acknowledgments—We thank Jill A. Priestley, Yibai Hao, Dr. Yu H. Hong, Dr. Cynthia J. DeLong, and Dr. Ryoko Ishida-Takahashi for advice and technical assistance.

REFERENCES

1. van der Donk, W. A., Tsai, A. L., and Kulmacz, R. J. (2002) *Biochemistry* **41,** 15451–15458
2. Rouzer, C. A., and Marnett, L. J. (2003) *Chem. Rev.* **103,** 2239–2304
3. Smith, W. L. (2008) *Trends Biochem. Sci.* **33,** 27–37
4. Schneider, C., Pratt, D. A., Porter, N. A., and Brash, A. R. (2007) *Chem. Biol.* **14,** 473–488
5. Herschman, H. R., Fletcher, B. S., and Kujubu, D. A. (1993) *J. Lipid Mediat.* **6,** 89–99
6. Tanabe, T., and Tohnai, N. (2002) *Prostaglandins Other Lipid Mediat.* **68,** 95–114
7. Kang, Y. J., Mbonye, U. R., DeLong, C. J., Wada, M., and Smith, W. L. (2007) *Prog. Lipid Res.* **46,** 108–125
8. Harris, R. C., McKanna, J. A., Akai, Y., Jacobson, H. R., Dubois, R. N., and Breyer, M. D. (1994) *J. Clin. Invest.* **94,** 2504–2510
9. Breder, C. D., Dewitt, D., and Kraig, R. P. (1995) *J. Comp. Neurol.* **355,** 296–315
10. Langenbach, R., Loftin, C. D., Lee, C., and Tiano, H. (1999) *Ann. N.Y. Acad. Sci.* **889,** 52–61
11. Smith, W. L., and Langenbach, R. (2001) *J. Clin. Invest.* **107,** 1491–1495
12. Yu, Y., Fan, J., Hui, Y., Rouzer, C. A., Marnett, L. J., Klein-Szanto, A. J., FitzGerald, G. A., and Funk, C. D. (2007) *J. Biol. Chem.* **282,** 1498–1506
13. Buchanan, F. G., Holla, V., Katkuri, S., Matta, P., and DuBois, R. N. (2007) *Cancer Res.* **67,** 9380–9388
14. Brown, J. R., and DuBois, R. N. (2005) *J. Clin. Oncol.* **23,** 2840–2855
15. Rouzer, C. A., and Marnett, L. J. (2009) *J. Lipid Res.* **50,** 529–534
16. Doller, A., Huwiler, A., Müller, R., Radeke, H. H., Pfeilschifter, J., and Eberhardt, W. (2007) *Mol. Biol. Cell* **18,** 2137–2148
17. Mbonye, U. R., Wada, M., Rieke, C. J., Tang, H. Y., Dewitt, D. L., and Smith, W. L. (2006) *J. Biol. Chem.* **281,** 35770–35778
18. Mbonye, U. R., Yuan, C., Harris, C. E., Sidhu, R. S., Song, I., Arakawa, T.,

and Smith, W. L. (2008) *J. Biol. Chem.* **283,** 8611–8623
19. Morita, I., Schindler, M., Regier, M. K., Otto, J. C., Hori, T., DeWitt, D. L., and Smith, W. L. (1995) *J. Biol. Chem.* **270,** 10902–10908
20. Morham, S. G., Langenbach, R., Loftin, C. D., Tiano, H. F., Vouloumanos, N., Jennette, J. C., Mahler, J. F., Kluckman, K. D., Ledford, A., Lee, C. A., and Smithies, O. (1995) *Cell* **83,** 473–482
21. Yang, P., Felix, E., Madden, T., Fischer, S. M., and Newman, R. A. (2002) *Anal. Biochem.* **308,** 168–177
22. Salmon, A. B., Murakami, S., Bartke, A., Kopchick, J., Yasumura, K., and Miller, R. A. (2005) *Am. J. Physiol. Endocrinol. Metab.* **289,** E23–E29
23. Aronoff, D. M., Peres, C. M., Serezani, C. H., Ballinger, M. N., Carstens, J. K., Coleman, N., Moore, B. B., Peebles, R. S., Faccioli, L. H., and Peters-Golden, M. (2007) *J. Immunol.* **178,** 1628–1634
24. Murphey, L. J., Williams, M. K., Sanchez, S. C., Byrne, L. M., Csiki, I., Oates, J. A., Johnson, D. H., and Morrow, J. D. (2004) *Anal. Biochem.* **334,** 266–275
25. Morrow, J. D., and Opp, M. R. (2005) *Brain Behav. Immun.* **19,** 28–39
26. Morrow, J. D., and Opp, M. R. (2005) *Brain Behav. Immun.* **19,** 40–51
27. Svenson, K. L., Bogue, M. A., and Peters, L. L. (2003) *J. Appl. Physiol.* **94,** 1650–1673
28. Chu, V., Otero, J. M., Lopez, O., Morgan, J. P., Amende, I., and Hampton, T. G. (2001) *BMC Physiol.* **1,** 6
29. Grosser, T., Fries, S., and FitzGerald, G. A. (2006) *J. Clin. Invest.* **116,** 4–15
30. Cheng, Y., Wang, M., Yu, Y., Lawson, J., Funk, C. D., and Fitzgerald, G. A. (2006) *J. Clin. Invest.* **116,** 1391–1399
31. Francois, H., Facemire, C., Kumar, A., Audoly, L., Koller, B., and Coffman, T. (2007) *J. Am. Soc. Nephrol.* **18,** 1466–1475
32. Liles, J. H., and Flecknell, P. A. (1992) *Lab. Anim.* **26,** 241–255
33. Li, S., Wang, Y., Matsumura, K., Ballou, L. R., Morham, S. G., and Blatteis, C. M. (1999) *Brain Res.* **825,** 86–94
34. Aronoff, D. M., and Neilson, E. G. (2001) *Am. J. Med.* **111,** 304–315
35. Aronoff, D. M., and Romanovsky, A. A. (2007) *Prog. Brain Res.* **162,** 15–25